Ferromagnetism induced in rutile single crystals by argon and nitrogen implantation

2009 J. Phys.: Condens. Matter 21 206002

(http://iopscience.iop.org/0953-8984/21/20/206002)

J. Phys.: Condens. Matter **21** (2009) 206002 (8pp) doi:10.1088/0953-8984/21/20/206002

Ferromagnetism induced in rutile single crystals by argon and nitrogen implantation

M M Cruz[1,2,5], R C da Silva[3,4], N Franco[3,4] and M Godinho[1,2]

[1] CFMC-Universidade de Lisboa, Campo Grande, Ed. C8, 1749-016 Lisboa, Portugal
[2] Departamento de Física, Faculdade de Ciências, Universidade de Lisboa, Campo Grande, Ed. C8, 1749-016 Lisboa, Portugal
[3] LFI, Departamento de Física, ITN, E.N.10, 2686-953 Sacavém, Portugal
[4] CFNUL, Avenida Professor Gama Pinto 2, 1649-003 Lisboa, Portugal

E-mail: mmcruz@fc.ul.pt

Received 12 January 2009, in final form 9 March 2009
Published 8 April 2009
Online at stacks.iop.org/JPhysCM/21/206002

Abstract

The magnetic properties of Ar- and N-implanted single crystalline TiO_2 rutile were studied and correlated with the induced disorder in order to clarify the influence of defects in the magnetic behaviour. Nominal fluences of 1×10^{17} and 2×10^{17} cm^{-2} and an implantation energy of 100 keV were used. The as-implanted single crystals exhibited ferromagnetic behaviour up to 380 K. Annealing at 1073 K induced recovery of the lattice structure and the decrease of the ferromagnetic moment in the case of Ar-implanted samples, but the magnetic moment did not change significantly for the samples implanted with nitrogen. No impurities, other than the implanted species were detected and consequently the ferromagnetic behaviour is attributed to defects created during implantation, which in the case of nitrogen remained in the lattice even after partial recovery of the structure.

(Some figures in this article are in colour only in the electronic version)

1. Introduction

The recent discovery of magnetism in oxides doped with nonmagnetic impurities opened up a new line of research in the study of room temperature ferromagnetic materials. The first systems exhibiting ferromagnetic behaviour without including magnetic elements were films of HfO_2 [1] and $Ca_{9.995}La_{0.005}B_6$ [2]. Since then, room temperature ferromagnetism (FM) has been observed in films of several oxides (TiO_2, In_2O_3, ZnO and SnO_2) [3–5] and attributed to the presence of structural defects in the film–substrate interface. Also in undoped oxide nanoparticles (CeO_2, Al_2O_3, ZnO, In_2O_3 and SnO_2) FM behaviour was observed and attributed to the presence of oxygen vacancies at the nanoparticles' surface [6]. In the case of undoped HfO_2 thin films, theoretical calculations indicate that cation vacancies are associated with stable magnetic moments and can induce FM [7]. In the case of ZnO thin films grown by pulsed laser deposition (PLD) the FM was attributed to Zn interstitials [3]. In a few studies on single-crystalline ZnO implanted with transition metals, the final doped configuration was shown to depend on the presence of defects [8–10]. To isolate the role of defects, single crystals of ZnO were implanted with argon, a nonmagnetic ion. The results indicate that also in this case ferromagnetic behaviour is obtained [11].

In TiO_2 there are several reports on defect-originated magnetism. Thin films of anatase and rutile TiO_2 deposited by PLD show a magnetic moment that was associated with oxygen vacancies [12]. This result is consistent with reported work on anatase films produced by PLD in $LaAlO_3$ substrates [13, 14] where a ferromagnetic signal was measured up to 880 K.

Although several mechanisms have been suggested as the source of ferromagnetism in these materials, a unique model cannot be put forward. Some results of band structure calculations indicate that exchange interaction between Ti^{3+} and Ti^{4+} can cause FM in anatase [14], but in TiO_2 films deposited on Si, reported x-ray photoelectron results

[5] Author to whom any correspondence should be addressed.

do not seem to support the presence of these ions, and Stoner exchange splitting of the Ti 3d band is considered the mechanism responsible for the FM behaviour. All these results were obtained in films where interfaces and substrates have an important role. Recent results obtained for polycrystalline rutile and rutile mixed with anatase indicate that oxygen vacancies are associated with the FM behaviour. Only Ti^{4+} ions were detected, excluding the Ti^{2+}–Ti^{3+} exchange mechanism as the origin of magnetic behaviour and proposing the existence of magnetic moments associated with the distorted electronic orbitals surrounding the oxygen vacancies [15]. To explain the ferromagnetism detected in the undoped oxides, the formation of a spin polarized defect band was proposed [16]. Recently it was reported that substitution of oxygen by nitrogen in insulating oxides can be sufficient to produce a diluted magnetic semiconductor (DMS) [17].

In this work, the magnetic properties of Ar- and N-implanted TiO_2 rutile single crystals are studied in order to evaluate the contribution of defects in the bulk oxide to the magnetic properties. The fact that defects are created in a single crystal avoids the dependence of surfaces and interfaces that strongly affects the results obtained for small particles or films. The comparison between the results obtained for argon- and nitrogen-implanted samples can give information about the mechanisms involved.

2. Experimental details

TiO_2 single-crystalline slabs cut parallel to (100) planes were implanted with 100 keV Ar ions, with fluences of 1×10^{17} and 2×10^{17} cm^{-2}, at room temperature. The energy of implantation was chosen in order to have the implanted ions at around 70 nm from the surface. Samples from the same batch were also implanted with N ions of the same energy and with a fluence of 1×10^{17} cm^{-2}. The implanted single crystals were subjected to annealing treatments at 1073 K, for 1 h, in order to promote lattice recovery and the rearrangement of the implanted ions. In each case the annealing atmosphere was chosen to be the gas of the implanted species in order to avoid possible loss of the implanted ions. To follow the damage induced by the implantation and the recovery behaviour of the host lattice after the annealing treatment, studies using Rutherford backscattering spectrometry (RBS), and RBS in combination with the channelling effect (RBS-C), were performed with a 2 MeV $^4He^+$ beam. The backscattered particles were detected at 140° and close to 180° to the incoming beam direction, with two silicon solid state detectors with 13 keV and 16 keV energy resolution, respectively. Proton-induced x-ray emission (PIXE) analysis was used to quantify the amount of implanted argon and to check for the presence of impurities in the unimplanted samples. X-ray diffraction (XRD) was performed with a high resolution double-crystal diffractometer in a θ–2θ geometry, using Cu Kα_1 radiation in order to access modifications in the implanted layer. XRD reciprocal space analysis was performed in a seven degree of freedom goniometer. To characterize the magnetic behaviour of the samples, magnetic moment measurements were carried out using a Quantum Design MPMS magnetometer, for applied magnetic fields up to 5.5 T and temperatures between 2 and 400 K. The magnetic moment was measured as a function of increasing temperature after cooling the samples from the highest temperature in zero field (zero-field-cooled, ZFC) or in the measurement field (field-cooled, FC). For all implanted samples, two experimental measurement geometries were used, with the external magnetic field parallel either to [010] or to [001] directions of rutile.

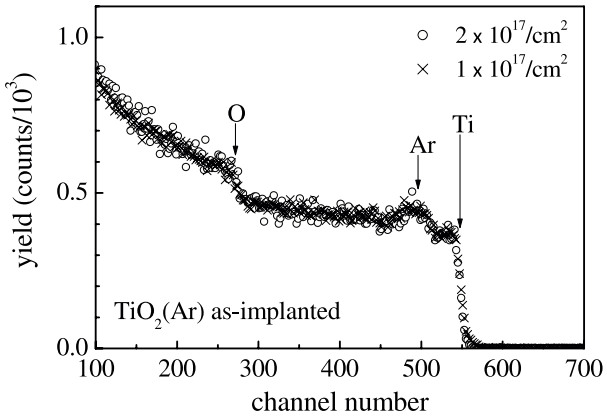

Figure 1. RBS-C spectra obtained for the as-implanted samples in a randomly oriented beam direction. Similar profiles were determined for the two nominal implanted argon fluences.

A careful characterization of the unimplanted single crystals allowed us to confirm that they display the expected Van Vleck paramagnetic behaviour of rutile [18] with an average magnetic susceptibility of 8.0×10^{-10} m^3 kg^{-1}, similar along the [010] and [001] directions. For the implanted crystals, the magnetic moment results are interpreted as the sum of two independent contributions: a paramagnetic component assigned to the unimplanted region of TiO_2 and the contribution of the implanted region. Since, in each case, the implanted depth corresponds to a very small fraction of the total sample volume (less than 0.1%), the paramagnetic moment of the unimplanted region was calculated using the measured susceptibility and the total mass. In order to isolate the moment of the implanted region this contribution was subtracted in all the experimental results. PIXE analysis revealed that no native impurities exist in concentrations above its experimental limit (of the order of 10^{-2}–10^{-3} at.% for all d-elements of the fourth and fifth periods); in particular, no magnetic impurities were detected.

3. Experimental results

3.1. Ar-implanted samples

3.1.1. As-implanted state. The RBS-C technique was used to study the implantation profiles and the damage induced in the TiO_2 lattice. Figure 1 shows the RBS results for the two implanted fluences, taken at a random incident direction, i.e. a direction that is not aligned with any major crystallographic direction. Due to the overlapping profiles of Ti and Ar, theoretical simulations using RUMP [19, 20] were performed in order to quantify the amount of implanted Ar.

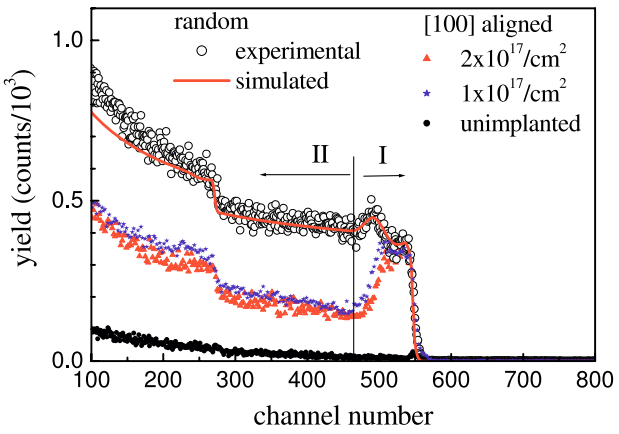

Figure 2. RBS-C spectra of as-implanted TiO_2(Ar) comparing the [100]-aligned spectra (triangles and stars) with a spectrum taken in a random direction (open circles) and also with a spectrum taken for a non-implanted surface (full circles). In the spectra region I corresponds to the implanted depth in Ti whereas II indicates a more profound region not affected by the implantation.

Consistent with the similarity of the two spectra, the results indicate that the retained fluence is of the order of 5×10^{16} cm^{-2} in both cases, extending to a depth around 125 nm. The fact that similar profiles are obtained for the two different fluences indicates that a saturation concentration was already attained at the lower fluence. Possibly argon diffuses away during the implantation. Sputtering may also be a contributing mechanism, especially during the higher fluence implantation. This would explain why the maximum of implanted concentration appears closer to the surface by about 30% for the sample implanted with higher fluence, 50 nm, as compared to 70 nm for the other fluence samples.

To study the damage produced by the implantation, RBS-C was carried out comparing the yields taken in different directions, in particular with the incident beam non-aligned versus aligned with the [100] crystalline direction of the rutile single crystal.

When the analysing beam is aligned with an axial direction, the steering of the incident ions by the long range periodic potential of the lattice structure gives rise to a dramatic reduction of the RBS yield. This reduction in the scattering yield is larger the better the crystalline quality and is an indication of the degree of damage in the host lattice.

Figure 2 presents the RBS results for the two implanted fluences, and also for the unimplanted TiO_2 for comparison. The high yield of the rectangular-shaped aligned spectra from the implanted region (I) as compared with those of the bulk, unimplanted region (II), and of the virgin unimplanted crystal, indicates a strong dechannelling of the host lattice due to a highly damaged implanted region extending to a depth of 125 nm.

Magnetization measurements of the as-implanted samples, at room temperature, indicate that a ferromagnetic component develops in both cases (figure 3). The saturation magnetic moment, obtained by extrapolating the high field regime for zero field, is higher for the sample implanted with the higher fluence in the [001] direction. This indicates that, in spite of

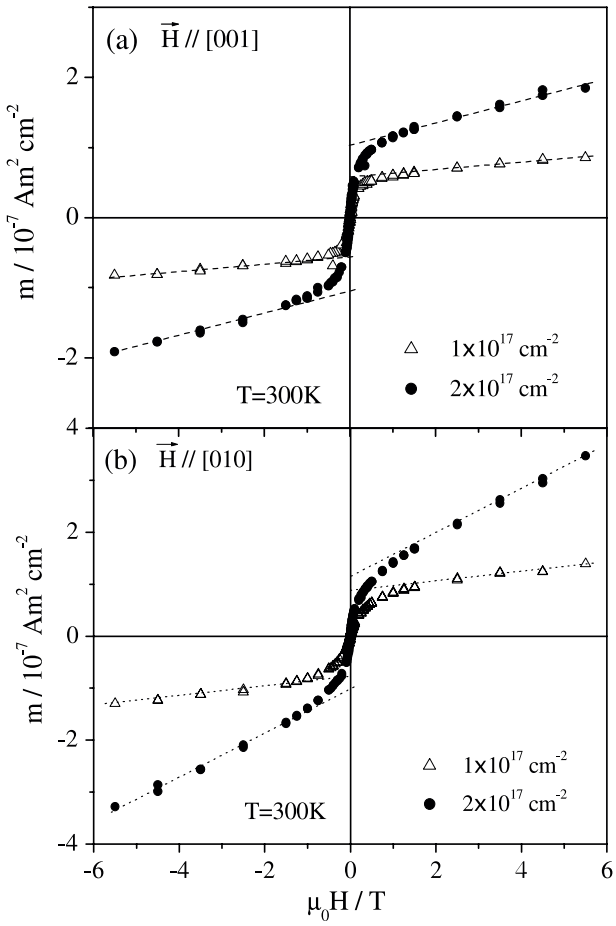

Figure 3. Hysteresis curves for samples implanted with 1×10^{17} and 2×10^{17} cm^{-2} argon nominal fluences, at $T = 300$ K, with the applied magnetic field (a) parallel to the c axis of rutile and (b) normal to the c axis of rutile.

the similar retained fluence, the higher fluence implantation modified the sample in a different way.

The values obtained at RT for the saturated magnetic moment density (per unit area) along the [001] direction are 6×10^{-8} A m^2 cm^{-2} and 1.1×10^{-7} A m^2 cm^{-2} for the samples implanted with nominal 1×10^{17} cm^{-2} and 2×10^{17} cm^{-2}, respectively. The saturation values are similar for magnetic fields applied along the [001] and [010] directions in the latter samples, while for the former, implanted with the lowest fluence, the results show magnetic anisotropy, with a saturated magnetic moment density of 8×10^{-8} A m^2 cm^{-2} along the [010] direction. The average values obtained correspond to magnetic moments of the order of 0.20 μ_B and 0.15 μ_B per implanted ion, for each implanted sample, respectively, considering the experimental value for the retained fluence, 5×10^{16} cm^{-2}.

If one assumes that the magnetic moment is associated with the damaged region extending for a depth of about 125 nm, the magnetic moments at 300 K correspond to 0.019 μ_B and 0.026 μ_B per unit formula for the samples implanted with nominal 1×10^{17} cm^{-2} and 2×10^{17} cm^{-2}, respectively.

Figure 4 illustrates the evolution of the magnetic moment density with temperature for one of the samples. The

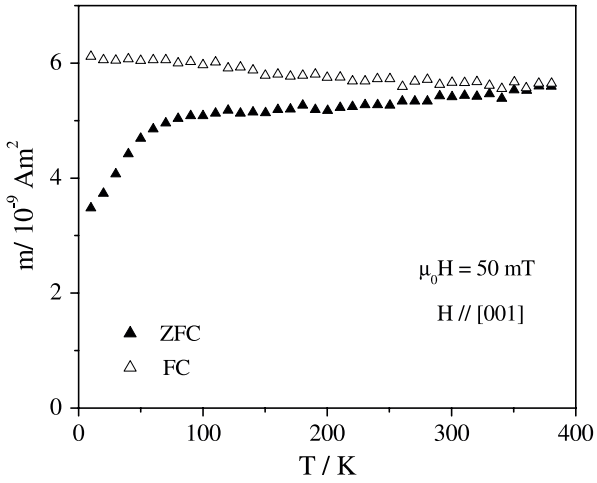

Figure 4. ZFC–FC curves for one sample implanted with 1×10^{17} cm^{-2} argon nominal fluence for applied magnetic field parallel to the *c* axis of rutile.

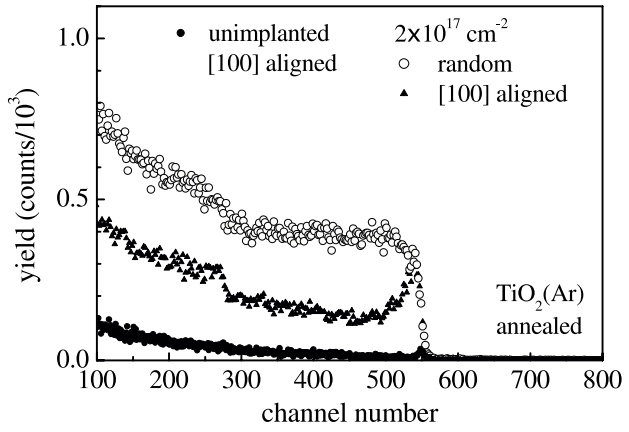

Figure 5. RBS-C spectra comparing the [100]-aligned (triangles) with a spectra taken in a random direction (open circles) and with an unimplanted surface (full circles) for a sample implanted with 2×10^{17} cm^{-2} argon nominal fluence after thermal treatment. Compare with figure 2 to see the effect of the annealing.

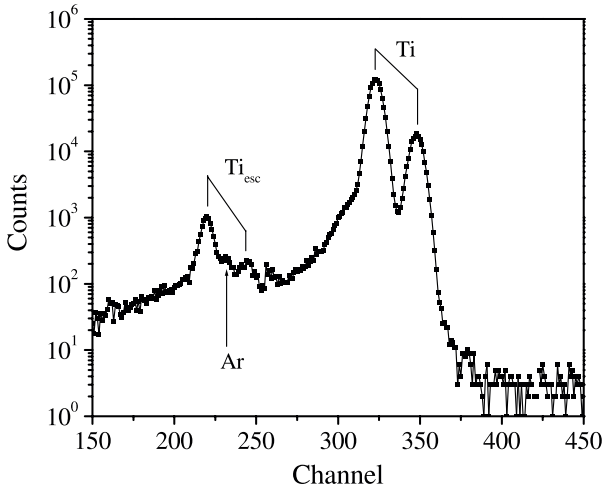

Figure 6. PIXE spectra for a sample implanted with 2×10^{17} cm^{-2} argon nominal fluence after thermal treatment.

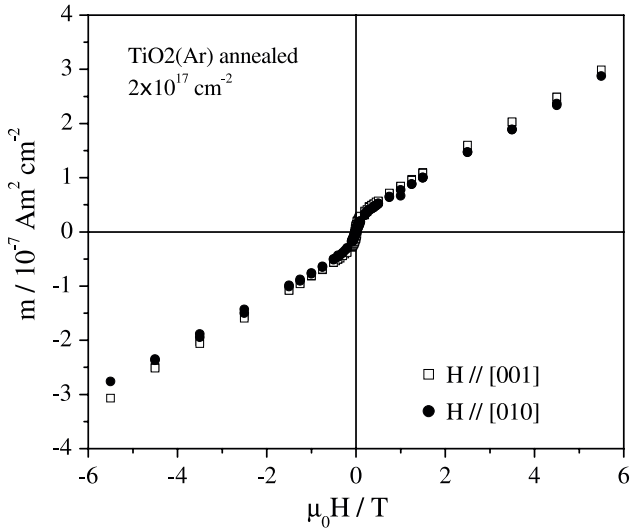

Figure 7. Hysteresis curves at $T = 300$ K for the sample implanted with 2×10^{17} cm^{-2} Ar nominal fluence after the annealing, measured parallel to the *c* axis of rutile (open squares) and along the [010] axis (full circles).

magnetic moment is almost constant up to 380 K with a small irreversibility observed at lower temperatures, indicating that the ferromagnetic behaviour is stable up to temperatures of 380 K.

3.1.2. Annealed samples. To recover the rutile structure and induce rearrangement of the implanted ions avoiding their loss, the samples were annealed at 1073 K in an Ar atmosphere for 1 h. After annealing the RBS spectra (figure 5) clearly show that the damage induced by the implantation procedure has been significantly removed.

The spectral data shows that the lattice recovers from the bulk to the surface region, corresponding to an epitaxial growth of the rutile lattice (compare figures 5 and 2).

The most damaged region extends in these samples to an average depth of 75 nm, about 60% of the as-implanted extent. RBS-C angular scans performed through the [100] direction, comparing the implanted and unimplanted face of the same crystal, indicate that the reminiscent damage is of the same type. To determine the retained fluence of Ar after annealing, PIXE analysis was used. The results indicate that Ar amounts to about 2×10^{16} cm^{-2} in the sample implanted with the higher fluence, indicating diffusion of Ar into the rutile structure (figure 6).

The magnetic behaviour of the samples changes after the annealing treatment. The samples still display a ferromagnetic behaviour (cf figures 7 and 8) but with a saturation magnetic moment only about 30% of the value determined for the as-implanted samples at 300 K.

The saturation moments measured are similar for the applied field parallel to the [010] and [001] directions, although lower than the values obtained for the as-implanted samples. The average value is now 3.5×10^{-8} A m^2 cm^{-2}. One of the characteristic features of these curves is the high value of

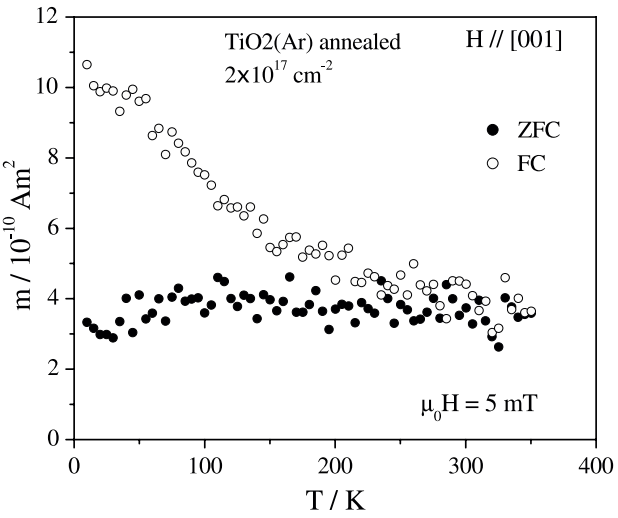

Figure 8. ZFC/FC magnetic moment measured at 5 mT for the sample implanted with 2×10^{17} cm^{-2} Ar nominal fluence after annealing.

the magnetic susceptibility observed up to 5 T. This value is higher in the case of the sample implanted with higher nominal fluence and can be explained by a small modification of the rutile susceptibility due to argon diffusion. The decrease of the ferromagnetic component after annealing, associated with the recovery of the lattice and annealing out of defects, is consistent with the idea that defects are at the origin of the ferromagnetic behaviour. In fact, the damaged region of rutile was reduced to a depth of 60% of that in the as-implanted state, and does not display the same rectangular-shaped profile, indicating that recovery also occurred, although only partially, in this region. To complement the information of the defect distribution in the lattice, XRD spectra in the reciprocal space were taken for a sample implanted with 2×10^{17} cm^{-2} (cf figure 9).

Figure 9 shows the reciprocal space maps (RSM) recorded around three different reciprocal lattice points, $(2, 0, 0)$, $(4, \bar{2}, 0)$ and $(4, 0, \bar{2})$. The most striking feature is the development of clear, well-defined truncation rods after annealing, i.e. characteristic distributions of diffracted intensities that are elongated along one direction. The (200) symmetric maps were collected with the diffraction plane parallel to (001), probing depth and lateral periodicity respectively along the [100] and [010] directions, while the $(4, \bar{2}, 0)$ asymmetric maps, collected with the same diffraction plane, mix the influence of [100] and [010] periodicity variations in the [240] direction. Variations in the periodicity of $(4\bar{2}0)$ spacing broadens the peak in the direction $[4\bar{2}0]$. To separately study the influence of disorder in the direction [100] the $(4, 0, \bar{2})$ maps were obtained with the diffraction plane parallel to (010). Clearly, the broadening in the $[40\bar{2}]$ direction (mixed effect of [100] and [001]) is smaller than the one obtained in the previous maps. Combining the results it is possible to conclude that the larger width of the diffraction peaks obtained after the annealing procedure is the result of a more disordered structure along the [010] direction.

These results are consistent with the observations by RBS-C that show that recovery of the crystalline order is not complete after annealing, leaving a significant residual damage, the deformation now detected in the RSM.

3.2. N-implanted samples

3.2.1. As-implanted state. Since nitrogen is a very light ion it is not possible to determine the implanted fluence either from RBS or PIXE. Nevertheless the RBS-C results displayed in figure 10 clearly show that the implantation resulted in an extended damaged region (∼300 nm). The implanted nitrogen extended to higher depths than Ar, the maximum concentration occurring at about 160 nm, but similar to argon-implanted samples the magnetization at room temperature displays a ferromagnetic behaviour (cf figure 11).

The saturation value is similar with the magnetic field applied along the [010] and [001] directions and amounts to 5.3×10^{-8} A m^2 cm^{-2}, 10% lower than the value obtained for the same nominal implantation fluence of argon. Since no experimental determination of the implanted fluence was possible, the nominal value was used to calculate the value per implanted ion, giving 0.07 μ_B. The temperature dependence of the magnetic moment density obtained at 5 mT is similar for both crystalline directions and is shown in figure 12 for the magnetic field parallel to [010]. The observed shape of the curve indicates the presence of nanosized magnetic aggregates with a blocking temperature close to 100 K. This possibility is confirmed by the observed decrease of about 25% in the saturation magnetization when increasing the temperature from 10 to 300 K.

3.2.2. Annealed samples. Similarly to the case of argon, N-implanted TiO_2 crystals were subjected to thermal treatments at 1073 K, for 1 h, but in a nitrogen atmosphere.

The RBS results (cf figure 13) show that the lattice recovers, but the type of rearrangement of the lattice is clearly different, corresponding not to an epitaxial growth of the lattice, as in the case of argon-implanted samples, but to a partial recrystallization recovery in the whole implanted region. The disordered region still extends to a length of 300 nm. The magnetic behaviour (figures 14 and 15) can be described by a ferromagnetic-like component added to a high susceptibility component, but no decrease of the saturation magnetic moment is detected when referred to the as-implanted state: values of 5–6 $\times 10^{-8}$ A m^2 cm^{-2} were obtained, irrespective of the direction of the applied magnetic field. This is in clear contrast with the case of argon-implanted samples. The ZFC/FC curves obtained after the annealing seem to indicate that aggregates are present in the lattice as for the as-implanted samples, but these aggregates have increased in size, as the blocking temperature is shifted to higher values, around 200 K. As in the case of argon implantation the slope at high fields can be explained by an increase of the TiO_2 susceptibility associated with the thermal treatment.

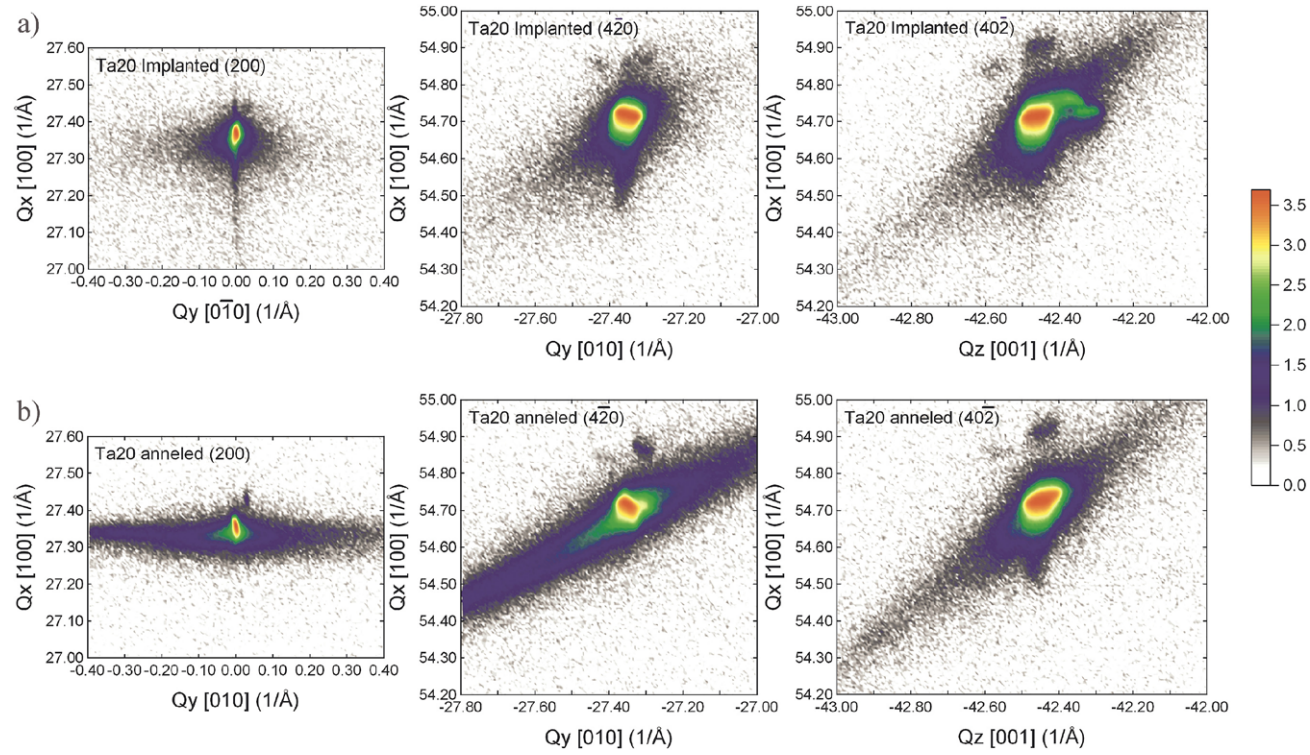

Figure 9. XRD analysis in reciprocal space for the sample implanted with 2×10^{17} cm^{-2} nominal fluence, exploring three space points, respectively (2, 0, 0), (4, $\bar{2}$, 0) and (4, 0, $\bar{2}$). (a) As-implanted sample and (b) annealed in argon at 1073 K. The colour scale represents a logarithmic scale of the intensity. The spot at higher Q_x in the RSM is merely a monochromator artefact.

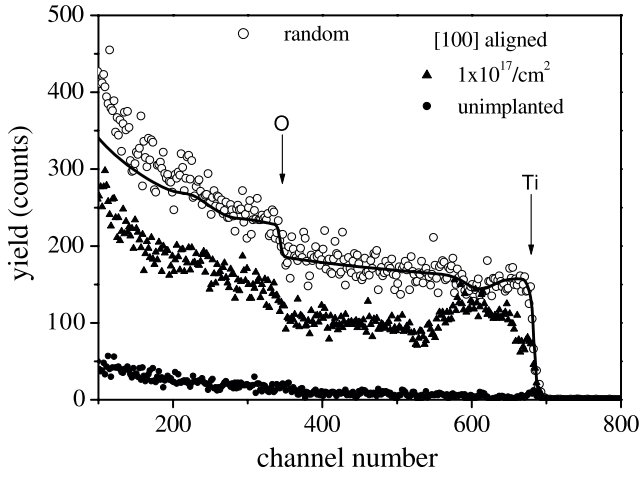

Figure 10. RBS-C spectra comparing the [100]-aligned (triangles) with a spectrum taken in a random direction (open circles) for a sample implanted with nitrogen with 1×10^{17} cm^{-2} nominal fluence and with an unimplanted surface (full circles). The solid line is the theoretical fit to random data.

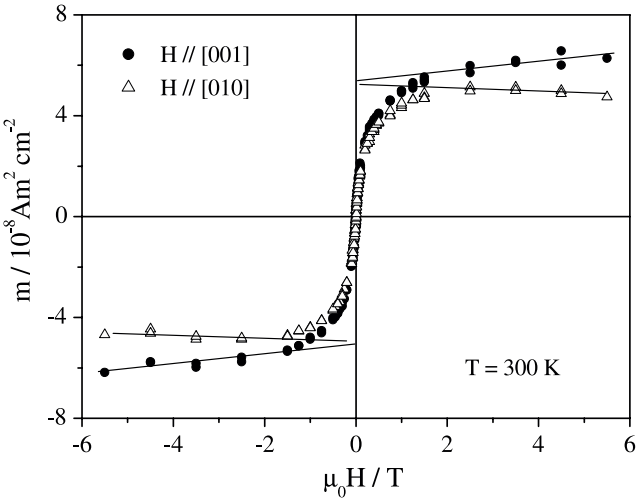

Figure 11. Hysteresis curves for a sample implanted with nitrogen with 1×10^{17} cm^{-2} nominal fluence at $T = 300$ K. The solid lines indicate the asymptotic behaviour and allow the determination of the saturation value as described in the text.

4. Discussion and conclusions

The results of this work clearly show that, after implantation of argon or nitrogen, both being nonmagnetic ions, TiO_2 rutile displays magnetic behaviour.

Magnetic defects associated with the implantation procedure could be the origin of the displayed ferromagnetic behaviour, since no impurities, magnetic or not, in concentration levels that may account for the observed magnetic behaviour, could be detected by PIXE, before or after implantation.

The Ti ions in the rutile lattice are surrounded by six oxygen ions in a distorted octahedral environment, implying that not only the fundamental state for two holes in the oxygen

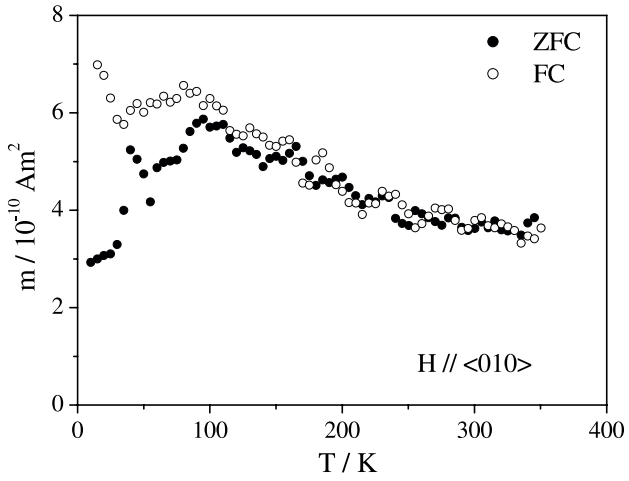

Figure 12. ZFC–FC curves for one sample implanted with nitrogen, 1×10^{17} cm^{-2} nominal fluence, for applied magnetic field parallel to the *b* axis of rutile.

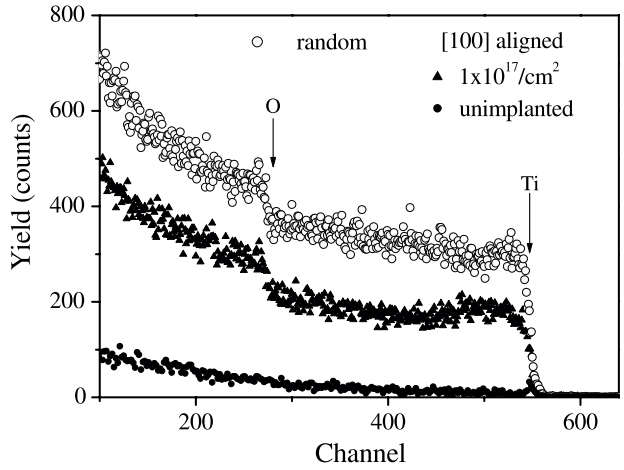

Figure 13. RBS-C spectra for a sample implanted with 1×10^{17} cm^{-2} nominal fluence of nitrogen after thermal treatment, comparing the spectra taken with [100]-aligned incidence (triangles) with a random incident direction (open circles). The aligned spectrum for an unimplanted surface (full circles) is also presented. Compare with figure 5 to see the effect of the annealing.

p-states around a Ti^{4+} vacancy can be a degenerate triplet giving rise to a magnetic moment [21], but also two-electron states in the neighbourhood of Ti atoms, located near to oxygen vacancies, will not have s-symmetry and can carry magnetic moment. This means that both Ti and O vacancies are defects that can have an associated magnetic moment. Interstitial Ti^{3+} ions will contribute with a paramagnetic signal.

Magnetic anisotropy is observed for the sample implanted with a lower fluence of argon, indicating that the orientation for the magnetization is favoured in the [010] direction. Considering this direction as the one for the majority of the point defects created, it would mean that the electronic deformation would preferably lie in this direction. This result is confirmed by the XRD results after annealing as shown in figure 9. If one considers that oxygen vacancies are the main magnetic defects, to have a deformation along the [010] direction, two neighbouring oxygen vacancies are required.

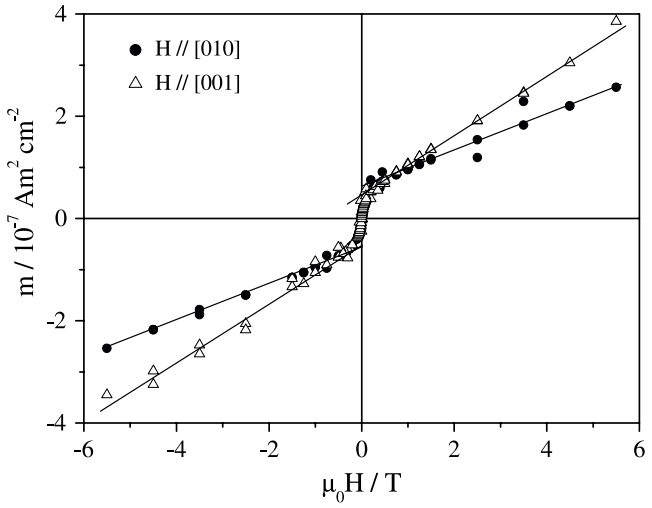

Figure 14. Hysteresis curves taken at 300 K for a sample implanted with nitrogen with 1×10^{17} cm^{-2} after thermal annealing.

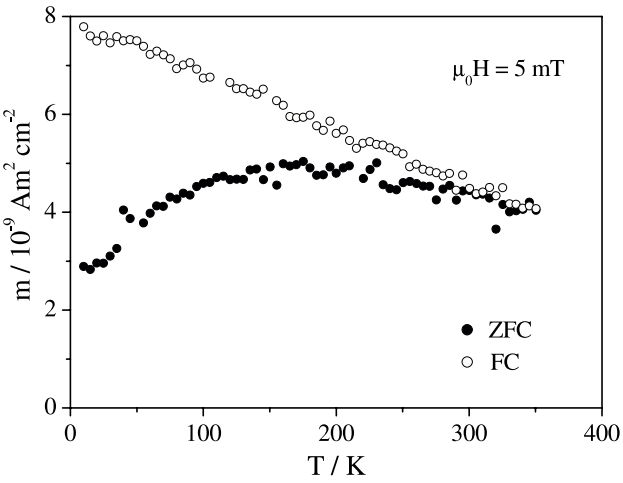

Figure 15. ZFC–FC curves for one sample implanted with nitrogen, 1×10^{17} cm^{-2} after thermal treatment, for applied magnetic field parallel to the *b* axis of rutile.

In the case of the implanted nitrogen samples, the recovery of the lattice is not accompanied by a decrease of the magnetic moment, indicating that the nitrogen-associated magnetic defect remains in the lattice. A possibility is a defect where nitrogen replaces oxygen in the octahedra surrounding Ti. This modification in the rutile lattice explains the different lattice recovery processes occurring in the nitrogen-implanted crystals when compared to the argon-implanted rutile. Density functional theory (DFT) calculations for nitrogen-doped anatase show that nitrogen doping reduces the energy cost for oxygen vacancy formation in bulk TiO_2 [22]. Since both rutile and anatase are composed of Ti surrounded by oxygen octahedra with similar Ti–O bond lengths, the same conclusion can be applied to rutile. Undoped rutile is easier to reduce than anatase [23], favouring the presence of substitutional nitrogen. Reductions of the energy cost for vacancy formation from 4.3 to 1.0 eV, and for oxygen substitution with nitrogen from 9.7 to 6.4 eV, were reported for rutile [22].

As N^{2-} has one electron less than oxygen, the binding energy of the 2p bonding electrons is lower than in the oxygen ion. This means that the N^{2-} ion has one electron in a state that will have a larger orbital radius than in an isolated ion. For a suitable concentration, the corresponding orbitals of the nearest defects will overlap, giving rise to a narrow impurity band with one hole per nitrogen ion exhibiting magnetic moment. Note that the lowest configuration for two holes in the 2p orbitals of oxygen or nitrogen is a spin triplet, implying the existence of an associated magnetic moment. One can estimate the binding energy of the hole to the nitrogen ion and the extension of the orbital in a simple way assuming a central potential, with $E = 13.6m^*/(\varepsilon_r^2 m_0)$ eV and $R = 0.0529\varepsilon_r m_0/m^*$ nm. Considering that the value of the dielectric constant for rutile is of the order of 150 [24] and the hole mass of the order of three times the free electron mass [25], $E \approx 1.8$ meV and $R \approx 2.6$ nm are obtained, implying that the overlap between nearby nitrogen ion orbitals would occur for concentrations of the order of 6×10^{19} cm^{-3}, i.e. 0.06 at.%, in the rutile structure. In our samples the implanted nitrogen extends to a depth of 160 nm with an average concentration of 6.25×10^{21} cm^{-3}, this value being about 100 times larger than the estimated threshold. This means that, although our calculation is oversimplified, it indicates that the implanted concentration is enough to have overlap between defect states and the formation of a defect band. In regions where the concentration is not large enough for this overlap to occur (in the tails of the implantation damage distribution), it is still possible to get magnetic clusters (regions with defects separated by well-crystallized rutile) as suggested by the obtained results.

In summary our results clearly demonstrate that magnetic defects in bulk TiO_2 rutile can be associated with lattice defects and not to any magnetic impurities. In spite of a small magnetic moment per unit formula the total magnetic moment of the implanted region does not change significantly from 10 to 350 K, indicating a strong interaction between the associated individual magnetic moments.

The number of defects created by argon implantation decreases after the annealing treatment and, in parallel, a reduction of the ferromagnetic moment occurs. Assuming that the majority of the defects are point defects, oxygen vacancies and Ti interstitials are considered responsible for the magnetic behaviour. By implanting nitrogen a different type of defect is obtained as it remains stable after thermal treatment, although lattice recovery is also observed. In agreement with theoretical results the substitution of oxygen by nitrogen is proposed. The high implanted concentration is associated with the appearance of a defect band responsible for the magnetism, indicating a possible route for the creation of DMS materials. The analogy between both behaviours prior to annealing supports the models that indicate oxygen vacancies as the main magnetic defects in undoped rutile.

Acknowledgments

We thank Dr L C Alves for the PIXE analysis. This work was carried out with the support of FCT through project PTDC/FIS/66262/2006.

References

[1] Coey J M D, Venkatesan M, Stamenov P, Fitzgerald C B and Dorneles L S 2005 *Phys. Rev.* B **72** 024450
[2] Young D P, Hall D, Torelli M E, Fisk Z, Sarrao J L, Thompson J D, Ott H R, Oseroff S B, Goodrich R G and Zysler R 1999 *Nature* **397** 412
[3] Hong N H, Sakai J and Brizé V 2007 *J. Phys.: Condens. Matter* **19** 036219
[4] Hong N H, Sakai J, Poirot N and Brizé V 2006 *Phys. Rev.* B **73** 132404
[5] Hong N H, Sakai J and Gervais F 2007 *J. Magn. Magn. Mater.* **316** 214
[6] Sundaresan A, Bhargavi R, Rangarajan N, Siddesh U and Rao C N R 2006 *Phy. Rev.* B **74** 161306(R)
[7] Chaitania Das P and Sanvito S 2005 *Phys. Rev. Lett.* **94** 217205
[8] Zhou S, Potzger K, Kuepper K, Grenzer J, Helm M, Fassbender J, Arenholz E and Denlinger J D 2008 *J. Appl. Phys.* **103** 043901
[9] Zhou S, Potzger K, Talut G, Reuther H, Kuepper K, Grenzer J, Xu Q, Mücklich A, Helm M, Fassbender J and Arenholz E 2008 *J. Phys. D: Appl. Phys.* **41** 105011
[10] Weyer G, Gunnlaugsson H P, Mantovan R, Fanciulli M, Naidoo D, Bharuth-Ram K and Agne T 2007 *J. Appl. Phys.* **102** 113915
[11] Borges R P, da Silva R C, Magalhães S, Cruz M M and Godinho M 2007 *J. Phys.: Condens. Matter* **19** 476207
[12] Rumaiz A K, Ali B, Ceylan A, Boggs M, Beebe T and Shah S I 2007 *Solid State Commun.* **144** 334
[13] Yoon S D, Chen Y, Yang A, Goodrich T L, Zuo X, Arena D A, Ziemer K, Vittoria C and Harris V G 2006 *J. Phys.: Condens. Matter* **18** L355
[14] Yoon S D, Chen Y, Yang A, Goodrich T L, Zuo X, Arena D A, Ziemer K, Vittoria C and Harris V G 2007 *J. Magn. Magn. Mater.* **309** 171
[15] Zhao Q, Wu P, Li B L, Lu Z M and Jiang E Y 2008 *J. Appl. Phys.* **104** 073911
[16] Coey J M D 2005 *Solid State Sci.* **7** 660
[17] Elfimov I S, Rusydi A, Csiszar S I, Hu Z, Hsieh H H, Lin H-J, Chen C T, Liang R and Sawatzky G A 2007 *Phys. Rev. Lett.* **98** 137202
[18] Senftle F E, Pankey T and Grant F A 1960 *Phys. Rev.* **120** 820
[19] Doolittle L R 1985 *Nucl. Instrum. Methods* B **9** 344
[20] Doolittle L R 1986 *Nucl. Instrum. Methods* B **15** 227
[21] Elfimov I S, Yunoki S and Sawatzky G 2002 *Phys. Rev. Lett.* **89** 216403
[22] Di Valentin C, Pacchioni G, Selloni A, Livraghi S and Giamello E 2005 *J. Phys. Chem.* B **109** 11414
[23] Bouzoubaa A, Markovits A, Calatayud M and Minot C 2005 *Surf. Sci.* **583** 107
[24] Parker R A and Vasilik J H 1960 *Phys. Rev.* **120** 1631
[25] Kasinski J J, Gomez-Jahn L A, Faran K J, Gracewski S M and Dwayne-Miller R J 1989 *J. Chem. Phys.* **90** 1253